BUTTERWORTH HEINEMANN

Polymer Vol. 36 No. 14, pp. 2699–2708, 1995
Elsevier Science Ltd
Printed in Great Britain
0032-3861/95/$10.00+0.00

The morphology and performance of holographic transmission gratings recorded in polymer dispersed liquid crystals

T. J. Bunning*, L. V. Natarajan, V. Tondiglia and R. L. Sutherland
Science Applications International Corporation, Dayton, OH 45431, USA

and D. L. Vezie†
LAI, 5100 Springfield Pike, Dayton, OH 45431, USA

and W. W. Adams
Wright Laboratory, Materials Directorate, Wright-Patterson AFB, OH 45433, USA
(Received 27 December 1994; revised 10 February 1995)

Holographic transmission gratings are formed by the anisotropic visible laser radiation curing of a multifunctional acrylate monomer blended with the liquid crystal (LC) mixture E7. This results in an anisotropic spatial distribution of phase-separated LC droplets within the photochemically cured polymer matrix. The morphology of thin films (5–20 μm) containing the gratings is examined by low-voltage, high-resolution scanning electron microscopy and transmission electron microscopy. Low concentrations of E7 (16% LC) coupled with rapid curing kinetics result in the formation of narrow LC-rich Bragg lamellae without well defined boundaries. These LC-rich lamellae, with approximate widths of 100 nm, are composed of small droplets measuring 20–50 nm in diameter. Increasing the concentration of LC in the prepolymer mixture results in larger lamellae (canals) of LC-rich material. Films formed from a mixture containing the highest LC concentration (34% LC) exhibited lamellae approximately 200–250 nm wide that are separated by polymer lamellae that also possess a small fraction of phase-separated LC droplets. The other variable examined in detail, laser writing intensity, has little effect on the morphologies exhibited in these films. The morphology is related to the performance (diffraction efficiency, transmission, switching times and fields) through a simple model.

(Keywords: phase separation; polymer dispersed liquid crystal; morphology)

INTRODUCTION

Interest in polymer-dispersed liquid crystal (PDLCs) systems has grown steadily since first described a decade ago[1,2]. Most of the attention has centred around switchable windows, films whose clarity can be varied from transparent to opaque by applying an electric field. Phase-separated droplets, wherein the anisotropic LC molecules conform to a configuration minimizing the free energy of the droplet, can be formed through a variety of techniques. If the droplet sizes are on the order of a micrometre in diameter, the spatial distortion of the refractive indices within the droplets results in a refractive index mismatch with its polymer host, which leads to a highly scattering film. The spatial arrangement of the refractive indices of these LC molecules can be modulated in a manner which eliminates scattering by the application of an electric field. Potential display applications and differences in preparation have been detailed[3,4].

The morphology of these isotropically cured systems has been examined using a variety of techniques, most notably optical microscopy and scanning electron microscopy (SEM)[5]. Two major types of phase-separated morphologies have been observed that are dependent upon the amount of LC employed. For lower concentrations, a 'Swiss cheese' morphology is exhibited, wherein spherical or ellipsoidal LC droplets are completely surrounded by polymer matrix. Microvoids left behind after removing the LC can be imaged by SEM. The second type of morphology consists of two continuous phases, one polymeric and the other LC, and has been described as a sponge-like morphology. This type of morphology is observed at higher concentrations of LC, typically greater than 50%, wherein connectivity among droplets is observed.

For a given LC concentration, the resulting LC droplet size can be controlled by varying the cure rate. In PDLC systems formed by polymerization, once the LC droplet has phase separated, its growth (and thus size) is governed by diffusion of LC from the rapidly growing polymer region into droplets. The droplet sizes and distributions are influenced by the diffusion of LC molecules and the relative propagation rate of the growing polymer, leading to gelation. Above a certain molecular weight and/or crosslink density, diffusion is

* To whom correspondence should be addressed
† Present address: The Gillette Company, One Gillette Park 6D-1, South Boston, MA 02127-1096, USA

slowed dramatically and the droplet size becomes fixed. Droplet diameters ranging from 0.02 μm to several micrometres have been obtained with a degree of control which allows optimization of specific electro-optical properties. Most scattering applications employ micrometre-sized droplets, which facilitate direct observation of the LC domains by optical microscopy. Droplets with sizes from 0.2 to 1 μm are typically imaged using conventional SEM after suitable preparation, including removal of the LC and the application of a conductive coating. Recent work examined the morphology of a u.v.-curable prepolymer mixture systematically as a function of concentration and curing intensity, using both SEM and polarized optical microscopy for very large LC domain sizes[6]. Very small droplets, less than 0.2 μm, have been imaged using TEM[7].

In the PDLC examples discussed previously, an isotropic distribution of LC droplets or domains in a polymeric host results. Several attempts to place LC domains spatially within these hosts have also been reported. Examples have included the use of a mask to introduce an intensity profile in the curing radiation, which results in spatially periodic LC domain sizes throughout a film[8]. High-intensity regions consist of primarily small-diameter droplets (due to the increased rate of polymerization which results in quicker gelation), while the lowest intensity regions possess the largest-diameter droplets. Spatially controlling the placement of LC in a polymer matrix, using surface relief gratings which are then back-filled with LC[9], has also been demonstrated. This technique produces films with alternating channels of polymer and LC. This multistep process of forming films is being examined as a means of producing switchable holographic gratings which have a wide range of application in diffractive optics. Another approach to overcome the limited performance of surface gratings is to back-fill periodic microscopic voids formed in a photochemically cured polymer system[10,11] to form volume gratings.

We have recently reported a method which combines the ease of photochemical curing with a spatially varying intensity profile to form films with alternating channels of polymer and LC[12–14]. The advantage of this technique is single-step fabrication of films with controllable droplet size, distribution of sizes, and widths of the polymer and/or LC channels. These gratings consist of periodic PDLC planes containing individual or coalesced LC droplets which have phase-separated in an anisotropic fashion (i.e. a grating). These films have high diffraction efficiency and low scatter, and can be electrically switched using low voltages.

We report here a discussion of the morphology of this system. Details of the preparation of these films have been given elsewhere[12,14]. Low-voltage high-resolution scanning electron microscopy (LVHRSEM) and transmission electron microscopy (TEM) were used to examine the anisotropically patterned texture. The effect of LC concentration and writing intensity on the phase-separation kinetics will be discussed, as observed by differences in the morphology of the surface and interior of these films.

EXPERIMENTAL

The materials and formation procedures of the diffraction gratings have been reported elsewhere[13]. In general, a complex mixture containing prepolymer, E7 liquid crystal (10–40%), photoinitiator ($M = 1.5 \times 10^{-3}$), chain extender (10%), and co-initiator ($M = 1.3 \times 10^{-1}$) is sandwiched between indium–tin oxide coated (ITO) plates. This mixture is cured using an Ar ion laser wherein, through the use of a prism, a spatial variation in the intensity across the sample is generated. The acrylate monomer employed is a penta-acrylate, which results in a very highly crosslinked matrix. LVHRSEM was performed using a Hitachi S-900 operated at 1.0 keV. Samples were lightly coated using a dual-ion-beam sputter-coater with 20–30 Å tungsten. Operation at this low accelerating voltage coupled with a thin conducting coating eliminates possible image artifacts caused by thick coatings (20–50 nm) employed at the higher voltages of conventional SEM. Samples were prepared by fracturing in liquid N_2 followed by a methanol extraction to remove the LC. After mounting on SEM stubs, samples were placed under vacuum to remove the methanol.

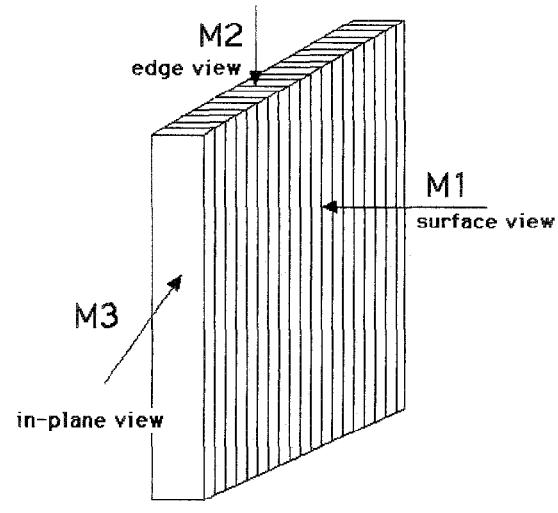

Figure 1 Schematic of thin film geometry showing orientation of grating relative to three viewing directions (M1, M2 and M3)

Three orientations were examined, as shown in *Figure 1*. The arrow direction corresponds to the viewing direction in the microscope. The surface morphology (M1) of the films was examined without a preference given to either side. Bulk fracture orthogonal to the grating direction (M2) allowed direct observation of the grating through the thickness of a film. Bulk fracture in a periodic plane of LC parallel to the lamellae direction (M3) allowed observation of the in-plane morphology resulting from the phase-separation process.

TEM samples were prepared by embedding films, with the LC still present, within epoxy and ultramicrotoming at room temperature. Sections were imaged using a JEOL 100CX TEM operating at 100 keV in the bright-field mode. Only sections microtomed perpendicular to the grating were examined (M2 viewing direction). Section thicknesses were approximately 800 Å. Grating spacings and film thicknesses were obtained using both LVHRSEM and TEM. Image analysis was performed by manually transforming the micrographs into binary data (black/white). The area fractions were determined using a Molecular Dynamics densitometer running ImageQuant software.

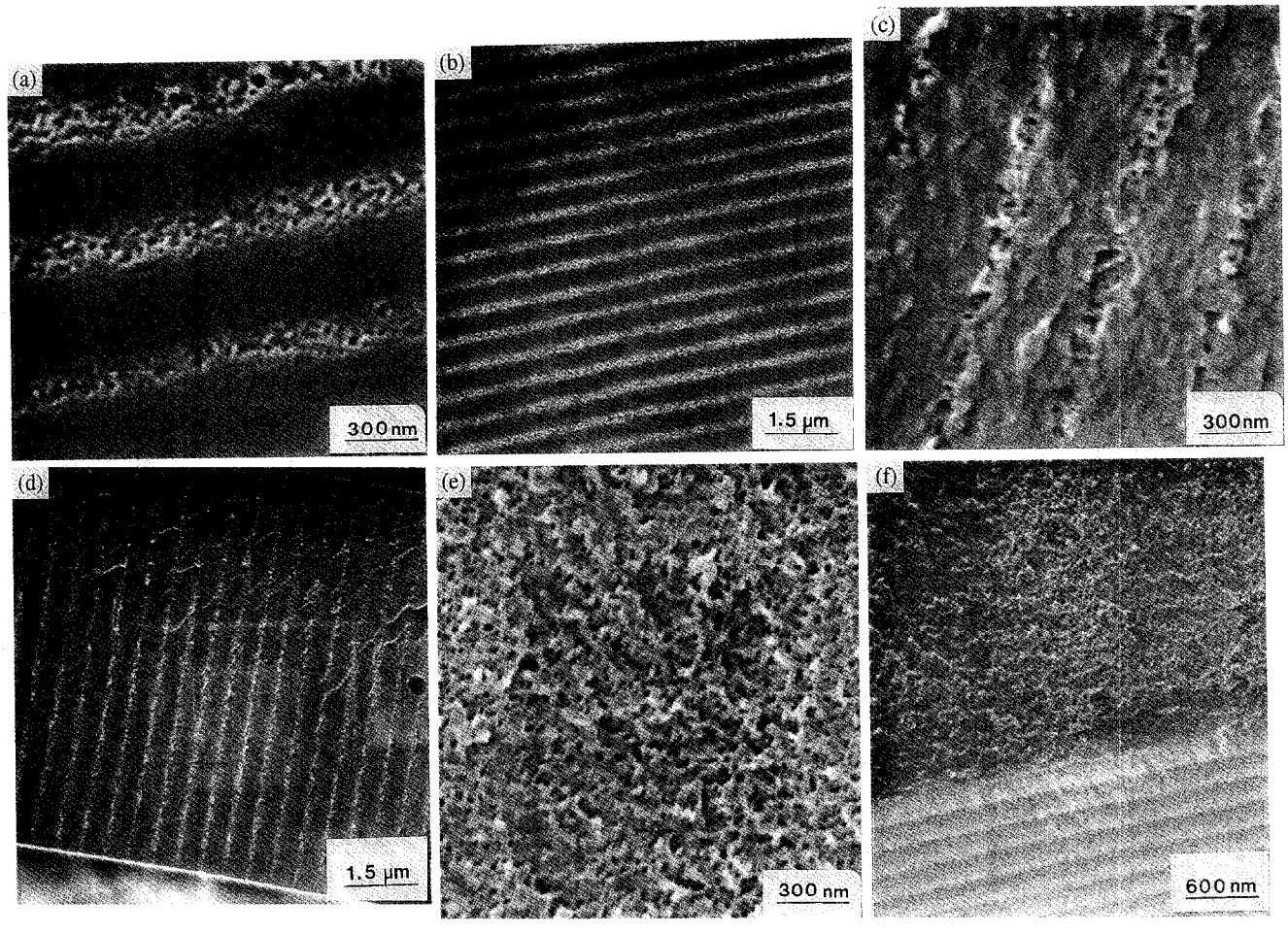

Figure 2 LVHRSEM micrographs of M1 (a,b), M2 (c,d) and M3 (e,f) orientations of grating recorded with 16% LC. Two magnifications for each orientation are shown

RESULTS AND DISCUSSION

A comparison of the morphologies of the three orientations shown in *Figure 1* can be seen from *Figures 2a–f* for samples containing 16 wt% LC. Each of the three orientations, M1, M2 and M3, is shown at low and high magnifications. LC-rich lamellae separated by dense crosslinked polymer are observed for the M1 and M2 orientations. A grating repeat (LC + polymer lamellae) of 0.56 μm is consistent with optical observations[13]. The LC-rich lamellae consist of small, spherical droplets with diameters ranging from 20 to 50 nm. The small diameters of these droplets indicate that once phase-separated, little growth occurs owing to the rapidly changing polymer molecular weight and high crosslink density. Both orientations (M1 and M2) indicate a polymer region with very few phase-separated droplets in between the LC-rich lamellae. The width of the LC-rich regions is considerably larger on the surface (M1) than in the bulk of the film (M2), as indicated by a comparison of *Figures 2a–d*. This behaviour was observed only at the surface, as uniform thickness LC-rich regions occurred through the bulk of these films. *Figure 2d* indicates the uniformity of the gratings through the thickness of the films. Parallel gratings, with little variability in the grating spacing, are observed.

The M3 orientation, shown in *Figures 2 e and f*, also indicates the presence of small droplets within the LC-rich lamellae, with sizes similar to those observed in the other two orientations. These images indicate a microstructure reminiscent of the Swiss cheese morphology observed in isotropically cured PDLC systems. Discrete droplets, averaging 30–50 nm in diameter with a small distribution of sizes and little connectivity, are phase-separated isotropically within the polymer matrix in the LC-rich regions. *Figure 2f* shows a film that has been tilted to allow a perspective which indicates the fracture path along the interior of a LC-rich plane.

The morphology of samples containing 34% LC, prepared with similar writing intensities to the 16% LC samples, is different, as shown in *Figures 3a–f*. M1 and M2 orientations indicate much wider LC-rich lamellae (200–250 nm) separated by a polymer-rich region. These LC-rich regions are not composed of discrete, spherical droplets but instead resemble canals of continuous LC, with a small amount of polymer bridging the canals. This structure is particularly evident in the surface orientations. These lamellae are present in the bulk of the film, although their width is again smaller than at the surface. *Figures 3c* and *d* indicate that a more granular structure is present in the polymer-rich regions as compared to the 16% LC samples. These M2 micrographs support the presence of a bicontinuous morphology in the LC-rich regions and some phase-separated droplets in the polymer-rich regions. M3 orientations (*Figures 3e* and *f*) from these samples show that two continuous phases are present within the LC lamellae. LC domain sizes ranging from 50 to 250 nm, with some connectivity

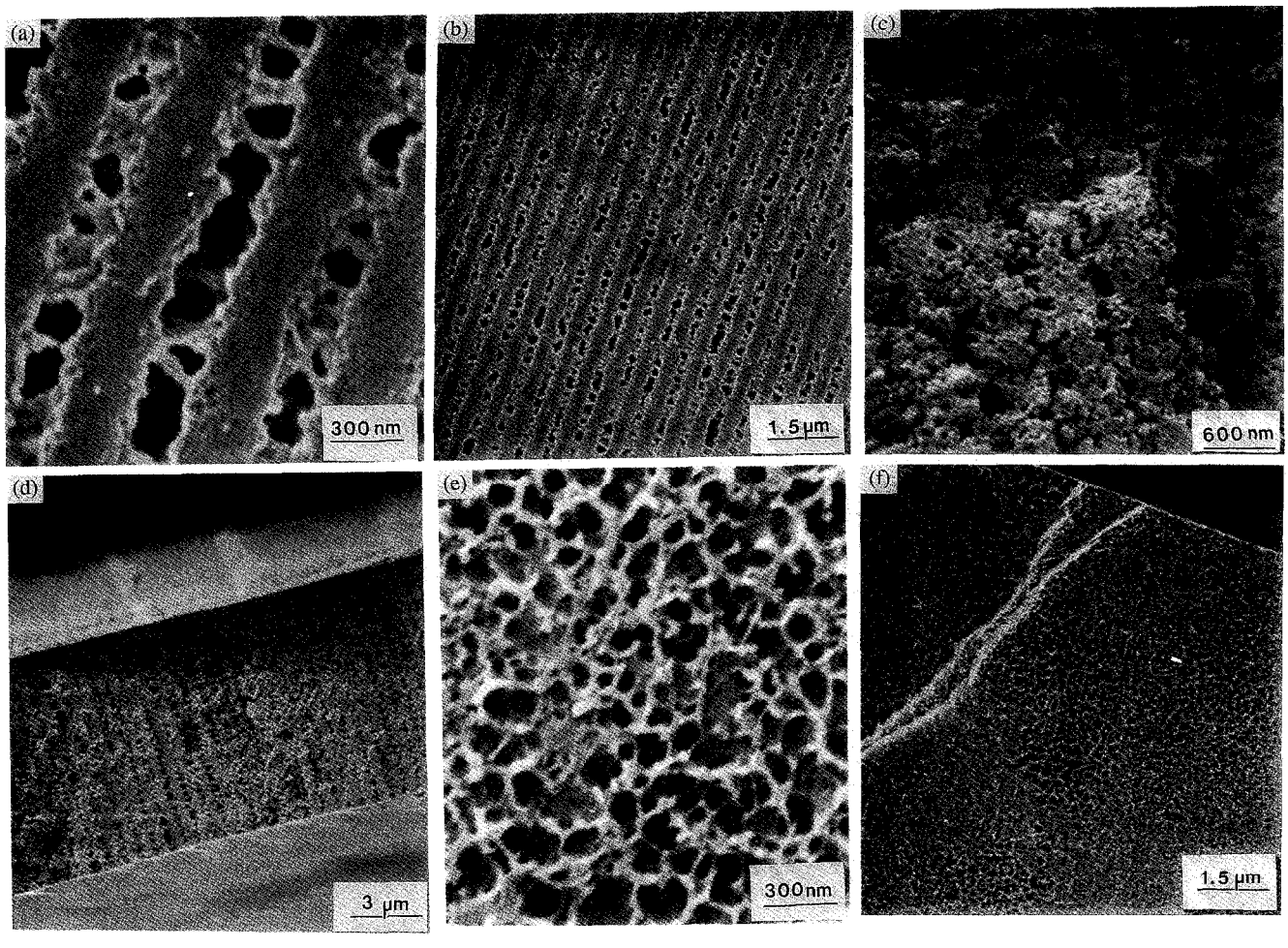

Figure 3 LVHRSEM micrographs of M1 (a,b), M2 (c,d) and M3 (e,f) orientations of grating recorded with 34% LC. Two magnifications for each orientation are shown

among the droplets, are observed coexisting within a continuous polymer matrix. This morphology, the sponge-like morphology, is typically observed for isotropically cured samples containing high concentrations of LC.

M3 orientations from films of both LC concentrations indicate a much larger volume fraction of droplets, as expected within the LC-rich lamellae compared to the bulk volume fraction. The area fraction of the microvoids was calculated from both M2 and M3 orientations and assumed to be approximately equal to the volume fraction. Because the LC phase-separates in an anisotropic manner, two separate volume fractions were obtained. The first, obtained from the M2 orientations, gives an indication of the 'global' volume fraction, that is the volume fraction of the LC droplets throughout the bulk of the films. These global fractions were approximately two-thirds the expected values (16% and 34%), indicating that some of the LC does not phase-separate, consistent with isotropic PDLC films[15,16]. The 'local' volume fraction was calculated from the M3 orientations and represents the fraction of LC residing within a LC-rich lamella. The fractions observed for the 16% LC and 34% LC samples were approximately 30% and 60%, respectively.

In an earlier, preliminary report on the electro-optic performance of some of these PDLC films, initial LVHRSEM micrographs from samples that had not been treated to remove the LC[13] showed dark regions spatially separated by dense polymer regions with a constant grating spacing. The dark regions were not spherical but instead were elongated along the grating, as shown in *Figure 4*. We now believe that these dark regions were formed by the LC material itself, which positively charges at these low accelerating voltages. The LC is drawn to the surface by surface tension and also possibly as a result of the high vacuum and beam heating encountered in the microscope. The confinement of elongated droplets along the gratings is caused by surface tension. Indeed, when compared to the images obtained here, wherein the LC has been removed, a considerable difference is observed, as shown by direct comparison of *Figures 4a* and *b*. After methanol extraction, microvoids appear dark owing to decreased secondary electron emission. The appearance of dark, shaded areas around microvoids attributed to LC domains has been previously[17] attributed to surface damage induced by the metallization of the samples. *Figure 4a* clearly indicates the presence of residual LC, which may be another explanation for these shaded areas.

TEM also supports the presence of bulk gratings through the thickness of a film, as shown in *Figures 5a* and *b* for systems containing 34% LC. Uniformity of the gratings across the thickness of the film is again observed. Alternating lamellae, composed of epoxy-rich and crosslinked polymer with a grating spacing of 0.56 μm, are observed. The width of the gratings and individual lamellae observed by TEM correspond well to

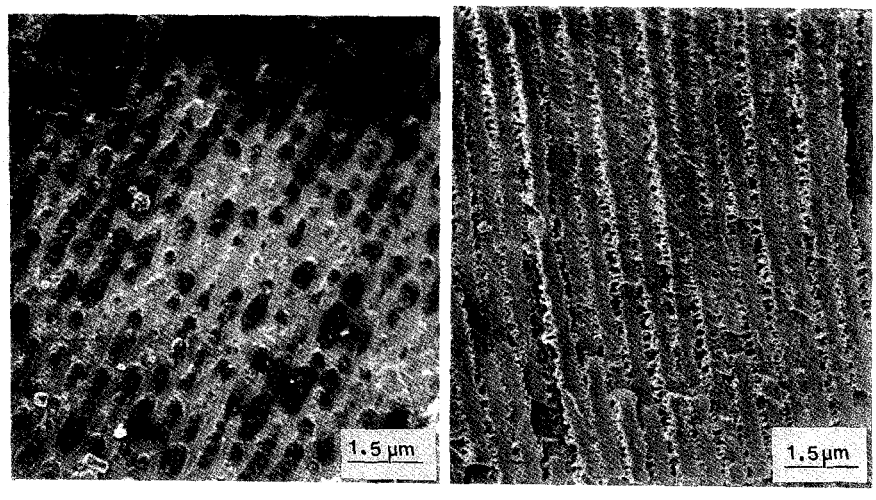

Figure 4 LVHRSEM micrographs of (a) sample not treated to remove LC, and (b) sample treated with methanol extraction to remove LC

those observed in the M2 orientation SEM micrographs. It is speculated that the epoxy monomer displaces the LC and is cured in the voids that were created by the phase-separation of LC. Volume fraction measurements of the TEM images yield results consistent with those obtained from the SEM images. Some contrast is evident in the polyacrylate polymer regions, which is consistent with the conclusion that a bicontinuous morphology is observed. Crosslinked polyacrylate regions can be seen bridging the epoxy-rich region in the higher magnification micrographs, consistent with the data observed in the LVHRSEM micrographs. Chatter is also evident, as a series of small, darker lines orthogonal to the grating planes in the polyacrylate regions was observed.

In the systems discussed above (16% LC and 34% LC), when grating morphology was examined as a function of writing intensity, no visible statistical differences in the width of the LC-rich lamellae and the range and frequency of droplet sizes were observed. Over two orders of magnitude in intensity (1 to 100 mW cm^{-2}) were studied. This behaviour is evident in *Figures 5a* and *b*, where two different laser intensities have been used to form the gratings. This behaviour can be contrasted to that observed from samples formed by expanding the laser beam so that constant spatial illumination across the sample was achieved. In this uniform illumination configuration, no gratings were recorded. As shown in *Figures 5c* and *d*, the higher intensity sample exhibited smaller domain sizes, consistent with previous work on conventional PDLC systems. Comparable intensities to those used in the formation of the gratings were employed for these flood-lit samples. Higher intensities result in less time for the droplets to grow by diffusion, because gelation occurs faster. Domains with average diameters ranging from 50 to 400 nm, compared to 250–600 nm, were observed for the flood-lit samples written at 80 mW cm^{-2} and 1 mW cm^{-2}, respectively. In addition, the morphology exhibited was different from that exhibited in the volume gratings, where small, nearly spherical droplets were observed. For the flood-lit samples shown in *Figures 5c* and *d*, a morphology with a high level of interconnectivity for both polymer and LC phases was observed. Speculation as to the significance of this difference in morphology will be discussed later.

This variation in morphology with laser writing intensity for flood-lit *versus* grating samples indicates that a fundamental difference in the process of phase separation of LCs occurs in isotropic *versus* anisotropic geometries. Considerable experimental and theoretical work[18,19] on anisotropic polymerization indicates that there is diffusion of monomer and other components consumed in the reaction towards the higher-intensity region. This gives rise to concentration gradients spatially across a film and through the depth of a film. The higher-molecular-weight polymer chains and oligomers migrate more slowly than the monomers, which results in the high-intensity regions being polymer-rich. These results can be extrapolated towards the system studied here, where an additional component, liquid crystal, is present. Ignoring interactions between various components, the chemical potential of the ith component of a mixture may be approximated by

$$\mu_i = \mu_i^0 + kT \ln\left(N_i \Big/ \sum_j N_j\right)$$

where μ_i^0 is the chemical potential of the pure ith component, N_i is the number of molecules of the ith component, j is the number of components, k is Boltzmann's constant, and T is the temperature[20]. Under thermodynamic equilibrium, μ_i = constant everywhere in the mixture. A gradient in the laser intensity preferentially initiates photopolymerization in the high-intensity regions. For components of the mixture which are consumed in this process, such as monomer molecules, the chemical potential in the high-intensity regions now decreases relative to that in the low-intensity regions. Conversely, for components which are not consumed, i.e. liquid crystal molecules, the chemical potential increases in the high-intensity regions over that in the low-intensity regions due to consumption of monomer molecules. Once formed, the polymer network is relatively immobile. Hence, there is diffusion of monomer and other reactants into the high-intensity regions and a diffusion of LC from the high-intensity regions as the system attempts to equalize chemical potentials everywhere and approach a new equilibrium state. As the polymer network propagates outward from the high-intensity regions due to extensive crosslinking, the molecular weight of the polymer grows, even in the

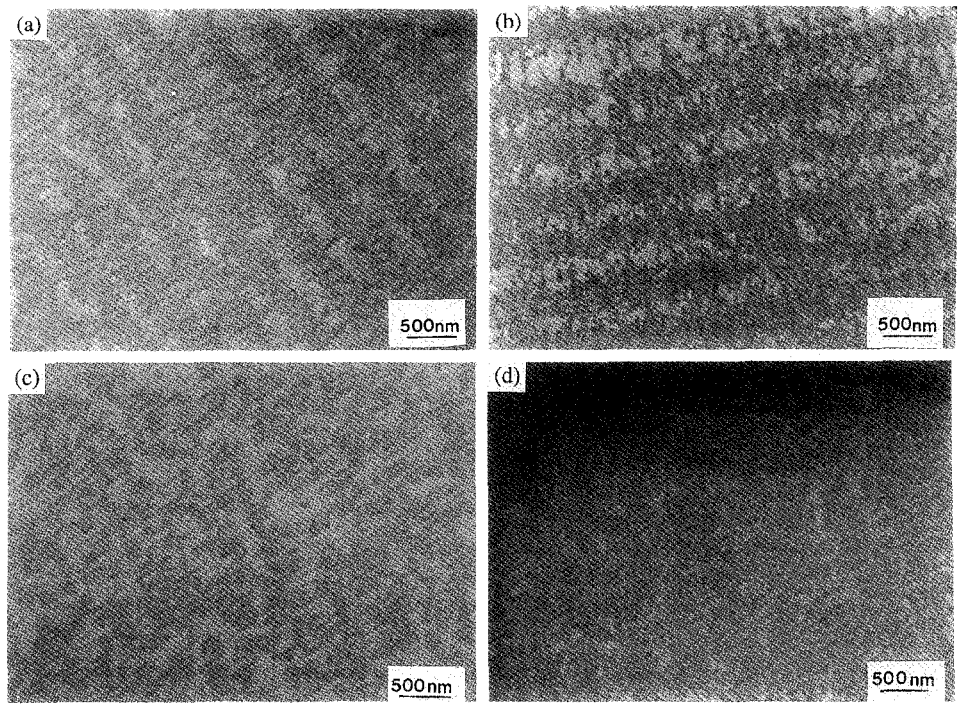

Figure 5 TEM micrographs of gratings written with 34% LC using 1 mW cm^{-2} (a) and 80 mW cm^{-2} (b) in addition to micrographs of flood-lit samples (35% LC) formed using a curing intensity of 1 mW cm^{-2} (c) and 80 mW cm^{-2} (d)

low-intensity regions. Eventually gelation is reached, at which point the LC is no longer miscible and separates as a distinct phase in the low-intensity regions. To minimize surface energy, the domains form as nearly spherical droplets. It is likely, however, that internal stresses slightly deform these droplets. When the local concentration of LC is higher, the probability of coalesence of these small domains is increased, and regions with large domains and some connectivity are observed, as in the 34 wt% LC samples.

The initial stage of phase separation is fundamentally different from that in isotropically cured systems, wherein no preferred direction for diffusion is present. The location of droplet phase separation is induced only by statistical fluctuations in an initially homogeneous mixture. Phase separation occurs by a mechanism dictated by the free energy/concentration diagram. For the anisotropically cured system, the forced diffusion of LC induced by the spatially varying molecular weight effectively increases the local fraction of LC in the low-intensity regions, as evidenced by the volume fraction measurements. This increased concentration in the region where phase separation occurs means that the stability of the system is based on a different location on the free energy/concentration diagram. Based on these differences, it is interesting to speculate that given the same starting composition, different types of phase separation behaviour may be induced for flood-lit (isotropically) *versus* anisotropically cured systems. Indeed, in the system discussed here, one may point out that the anisotropically cured system exhibits very small droplets (nearly spherical) which have had little time to coarsen due to the fast photopolymerization. This behaviour is consistent with that of an emerging phase from a nucleation and growth phase separation, wherein small, spherical droplets form in the early stages and then continue to grow[21]. This morphology may be directly compared to the flood-lit sample morphology, which resembles more an early-stage spinodal decomposition system; with a high degree of interconnection among phases[22]. Both of these observations are speculative; only evaluation of the structure factor in real-time can be used to fully understand the phase-separation behaviour. However, the introduction of forced diffusion needs to be considered in these systems, as it adds another variable in the already complex phase-separation behaviour.

The above explanation suggests that an induction period is present wherein the LC diffuses spatially more or less in one direction. If enough time is allowed, all the LC can be expected to diffuse into the low-intensity region and, upon phase separation, a step function in the distribution of polymer and LC regions would be expected. If the rate of polymerisation greatly exceeded the diffusion time, then no anisotropic distribution in the location of LC would be expected. While not completely resembling a step function, the gratings observed in this work clearly are well-defined spatially, indicating that sufficient time is present for the LC to diffuse. Real-time examination of the development of the gratings, using He–Ne radiation of these films, indeed supports the idea that an induction period in the growth of the diffraction efficiency is present, as shown in *Figure 6*. The observation of measurable diffraction efficiency (< 1%) assumes that droplets must have phase separated anisotropically, thereby forming a gradient in the refractive index. A variable refractive index profile across the film, due only to the spatially varying molecular weight of different polymer molecules, has been observed to account for up to a 1% diffraction efficiency. As indicated in *Figure 6*, a period where little change is evident is followed by a sharp increase in the

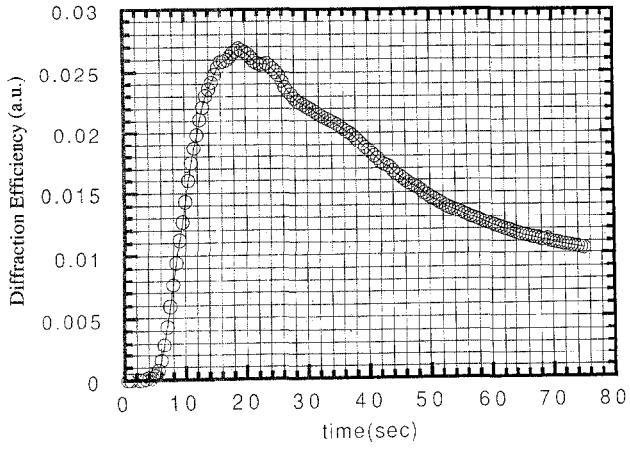

Figure 6 Diffraction efficiency *versus* time monitored using a He–Ne probe during the anisotropic curing process

diffraction efficiency (>1%) due to the formation of LC domains in a regular spatial pattern. The decrease of the efficiency after a finite time is due to increased scattering of larger droplets. If the induction period is longer than the time to diffuse approximately one-half of a grating spacing, anisotropic structures will occur, wherein there is very strong local confinement of the nucleated LC droplets. For example, the apparent induction time shown in *Figure 6* is on the order of 5 s. A diffusion over 0.28 μm (i.e. half the grating spacing) in this time places a lower limit on the diffusion coefficient of $D \approx 10^{-10}\,cm^2\,s$. Actual diffusion coefficients, before gelation occurs, of two to four orders of magnitude greater than this are not unreasonable. Initial work on samples with gratings of much larger Bragg spacings indicates less confinement of phase-separated droplets to a narrow region; instead, a larger distribution in the frequency of distribution across the entire spacing was observed. An increase in the Bragg spacing decreases the probability that all LC molecules can diffuse over one-half this distance given similar polymerization kinetics. Therefore, although the same volume fraction of LC domains may exist, they are less likely to be as narrowly confined in larger *versus* smaller Bragg spacing samples.

Table 1 summarizes the droplet sizes and periodic LC-rich plane widths as a function of both LC concentration and writing intensity. As shown, some of these films have good electro-optical performance, as indicated by transmission and critical fields for electrical switching. The critical fields were determined by fitting the field-dependent diffraction efficiency data to a model described below. Consistent with the morphological observations, little difference in these parameters was observed with writing intensity, while a large difference was observed with respect to LC content. The performance of these films can be defined as shown in *Figure 7*. The incident light (at the Bragg angle) can be either

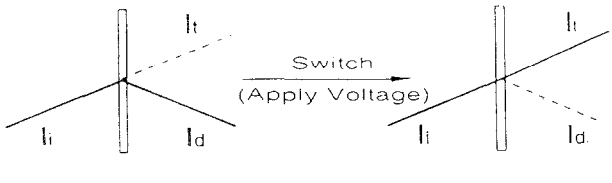

Figure 7 Definition of incident, transmitted and diffracted radiation

Table 1 Droplet sizes and periodic LC-rich plane widths as a function of both LC concentration and writing intensity

Sample	%LC	Intensity (mW cm^{-2})	Surface LC width (nm)	Edge LC width (nm)	Droplet diameter (nm)	% Trans. (P) @ 0 V	%DE (P) @ 0 V	% Trans.+ %DE	Critical field (V μm^{-1})
A	16	66	120–150	110	30–50	70	9.4	79.4	50
B	34	68	250–300	200–250	200–250	5.2	52.7	57.9	10.5

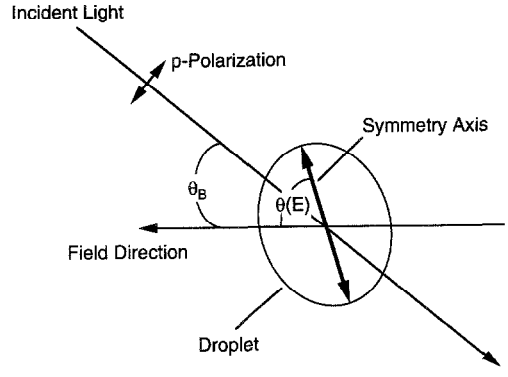

Figure 8 Schematic of ellipsoidal PDLC droplet interacting with a low-frequency electric field and a *P*-polarized field incident at the Bragg angle θ_b

diffracted or transmitted, depending on the presence or absence of a refractive index grating through the bulk of the samples, in this case formed by varying channels of LC-rich and polymer-rich material. Manipulation of the refractive index mismatch with an electric field allows switching to occur. The morphology of these films is related to the switching characteristics of these films, as the strengths of the electric field and the optical properties of these films are governed by the size and distribution of the LC droplets.

The overall transmissive properties are much better for the 16% LC samples, as evidenced by the values listed in the *%trans* + %DE column of *Table 1*. The *P* signifies *P* polarization, and differences between *P* and *S* polarization have been discussed previously[12,13]. The difference between these values and 100% transmission is attributed to random optical scattering and, as shown, the 34% LC samples exhibit 25–30% more scatter than the 16% LC samples. This behaviour is consistent with the smaller domain sizes exhibited by these samples and the fact that the 34% samples exhibit a sponge-like morphology in the LC-rich regions.

It is interesting to correlate the electro-optical behaviour of these gratings to the observed microscopic morphology. To this end, a simple diffraction model was developed. The medium is assumed to have a periodic step-index profile, with low index regions being polymer, and high index regions having some effective index determined by the local volume fraction of LC. To apply Kogelnik's coupled-wave theory[23], which assumes a sinusoidal index modulation, the first Fourier coefficient of the fundamental cosine term in the Fourier expansion of the step-index profile was computed, based on the width of the LC-rich region relative to the grating spacing. This coefficient was then used to compute the index modulation amplitude, and a sinusoidal modulation was used as an approximation to the step-index profile. Other information required is the effective LC droplet index relative to the surrounding polymer matrix index. This is not completely known since some fraction of the LC remains dissolved in the polymer, modifying its refractive index. However, the main interest here is the switching behaviour of the gratings and not their absolute diffraction efficiencies. By normalizing the diffraction efficiency to the peak value (at low voltages), the results of the model become relatively insensitive to the actual values of the refractive indices. What remains critical is the birefringent behaviour of the LC domains and their reorientation to an applied electric field.

As mentioned earlier, internal stresses may be at work during the curing process to slightly distort and elongate the droplets. This would have the effect of creating a preferred symmetry axis for alignment of the nematic director field along the long droplet axes, creating what is known as the bipolar droplet configuration[24]. The effective droplet index along this symmetry axis, $n_{\parallel}$ (the extraordinary index), is larger than that perpendicular to this axis, $n_{\perp}$ (the ordinary index). Correspondingly, there is a low-frequency dielectric anisotropy which results in a torque on the droplet when an external electric field is applied, attempting to reorient the droplet axis to the field direction. Counteracting this is a shape-dependent elastic torque which seeks to minimize the free energy in the absence of the applied field by restoring the symmetry axis to its position along the long axis of the droplet. The geometry of the configuration is illustrated in *Figure 8*, where the elongation of the droplet has been exaggerated for illustration.

Treating individual LC domains as uniaxial droplets in a bipolar director configuration, the droplet refractive index can be written as:

$$n_{LC} = \frac{n_{\parallel}}{\{1 + (\Delta n/n_{\perp})^2 \cos^2[\theta(E) - \theta_B]\}^{1/2}} \quad (1)$$

where $\Delta n = n_{\parallel} - n_{\perp}$ is the droplet birefringence, θ_B is the angle of incidence of the light (the Bragg angle), and $\theta(E)$ is the field-dependent angle of the droplet symmetry axis with respect to the applied field. It is assumed that $n_{LC} > n_{polymer}$ for all angles, so the minimum index modulation, and hence the minimum diffraction efficiency, will occur when $\theta(E) = \theta_B$, i.e. when the droplet symmetry axis is aligned along the direction of the incident light. Therefore, as the droplet symmetry axis is rotated to align with the field normal to the plane of the film, the diffraction efficiency will go through a minimum.

As mentioned above, the normalized diffraction efficiency is not very sensitive to the actual values of $n_{\parallel}$, $n_{\perp}$ and Δn, but the field dependence of the symmetry axis orientation is important. This dependence will be determined by a balance between the electric and shape-dependent elastic torques that minimize the free energy density of the droplet, which is related directly to the local droplet curvature. Applying a model due to Wu *et al.*[24], the droplets are assumed to have an elongated form with semi-major and semi-minor axes of *a* and *b*, respectively. The radius of curvature ρ of the droplet is given by:

$$\rho = a\{\cos^2[\theta(E) - \theta_0] + l^2 \sin^2[\theta(E) - \theta_0]\}^{1/2} \quad (2)$$

where $l = a/b$ is the droplet aspect ratio, and θ_0 is the angular orientation of the droplet at zero field. For aspect ratios close to 1, the droplet shape modelled by equation (2) is approximately ellipsoidal. The balance of field and elastic torques yields the field-dependent orientation angle:

$$\theta(E) = \tfrac{1}{2}\tan^{-1}\left(\frac{\sin 2\theta_0}{\cos 2\theta_0 + E/E_c}\right) \quad (3)$$

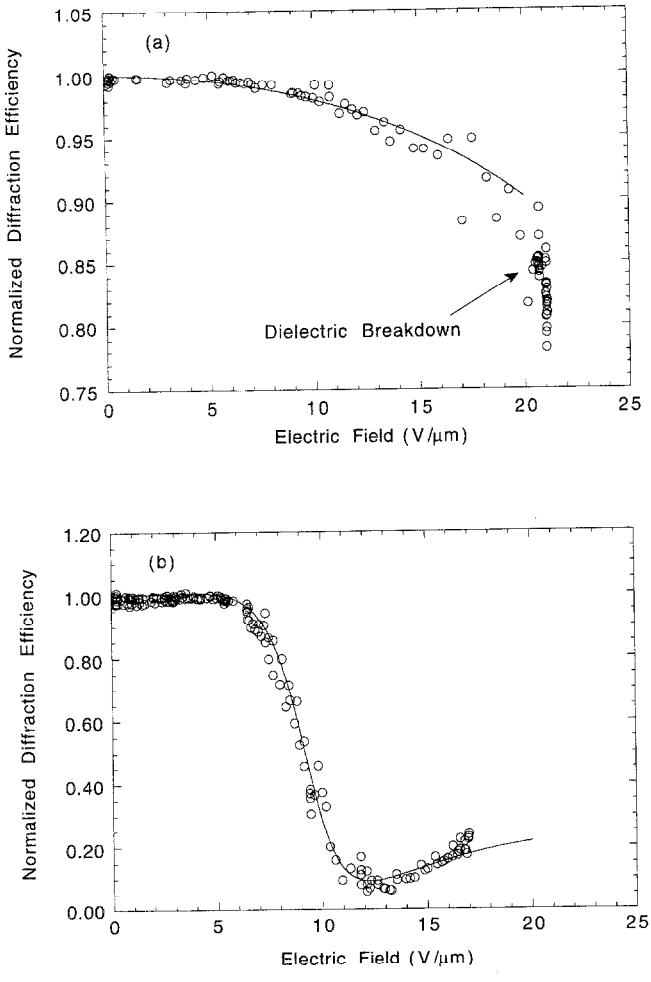

Figure 9 Normalized diffraction efficiency as a function of applied electric field for (a) 16% sample and (b) 34% sample. The circles are data and solid curves are fits of the model discussed in the text, with critical fields (a) $E_c = 50\,V\,\mu m^{-1}$ and (b) $E_c = 10.5\,V\,\mu m^{-1}$

where a critical field E_c is defined by:

$$E_c = \frac{1}{3a}\left(\frac{\sigma_{LC}}{\sigma_p} + 2\right)\left[\frac{k_{33}(l^2 - 1)}{\Delta\epsilon}\right]^{1/2} \quad (4)$$

In this equation, σ_{LC} and σ_p are the low-frequency conductivities of the LC and the polymer, respectively, while k_{33} is the elastic bend force constant and $\Delta\epsilon$ is the dielectric anisotropy of the LC.

Diffraction efficiency as a function of applied field is given in *Figures 9a* and *b*, respectively, for the 16% and 34% samples. The solid curves are a fit of the diffraction efficiency η given by Kogelnik's theory:

$$\eta = \sin^2 \kappa L \quad (5)$$

where L is the sample thickness, and $\kappa \propto (n_{LC} - n_{polymer})$ is the coupling coefficient. Thus, the coupling coefficient is determined by equations (1) and (3), and two parameters strongly influence the shape of the field-dependent diffraction efficiency curves: θ_0 and E_c.

For both of the theoretical curves in *Figures 9a* and *b*, $\theta_0 = 0.42\pi$ was selected. Most notably in the 34% LC sample, the sharpness of the knee of the curve, where the diffraction efficiency rolls over and begins to decrease, is a sensitive function of this initial angle. This seems to be an indication that the droplet axes are initially aligned preferentially along a direction nearly parallel to the grating vector. The fact that *P*-polarized light is more strongly diffracted at zero field[12,13] is in agreement with this implied orientation. No difference was observed in the diffraction efficiency after curing with two different polarizations, thereby eliminating light-induced alignment of the LC during curing. The strong polarization dependence[12,13] observed with LC content arises from differences in the domain shapes (droplets *versus* lamellae) and the associated surface anchoring of the LC molecules. The anisotropic flow and growth of the polymer chains during photopolymerization is thought to be a primary factor in dictating this behaviour.

The critical fields for the 16% and 34% LC samples used in the model calculations are 50 and $10.5\,V\,\mu m^{-1}$, respectively, as listed in *Table 1*. Further substantiation of this simple model is given by estimations of the critical field using equation (4). For the LC E7, $k_{33} = 19.5 \times 10^{-12}$ N and $\Delta\epsilon = 14.5\epsilon_0$ (ref. 25), where ϵ_0 is the vacuum permittivity. Taking a reasonable estimate of $\sigma_{LC}/\sigma_p = 25$ (ref. 24), a very modest aspect ratio, $l = 1.05$ (nearly spherical droplets), and average droplet sizes $a = 0.02\,\mu m$, and $a = 0.113\,\mu m$ for the 16% LC and 34% LC samples, respectively, the values of E_c calculated using equation (4) are 56 and $10\,V\,\mu m^{-1}$. The model fits the experimental data remarkably well, as shown in *Figures 9a* and *b*. Note that the data indicate that the critical field for switching scales inversely with the droplet size, in agreement with equation (4).

It is interesting to further examine the response time for switching predicted by this simple model. Wu *et al.*[24] show that the turn-off time is given by:

$$\tau_{off} = \frac{\gamma_1 a^2}{k_{33}(l^2 - 1)} \quad (6)$$

where γ_1 is the rotational viscosity of the LC. Generally, this is larger than the bulk viscosity. Assuming that γ_1 is as much as a factor of three to five times larger than the bulk viscosity, which is $0.039\,kg^{-1}\,s^{-1}$ for E7, equation (6) predicts sub-millisecond turn-off times for both droplet sizes. Preliminary investigations of response times for diffraction efficiency switching in these materials indeed indicate sub-millisecond response.

Finally, it is noted that, in agreement with the data for the 34% sample, the model does predict that the diffraction efficiency goes through a minimum as the applied field is increased. This corresponds to the situation where $\theta(E) = \theta_B$, as discussed above. Thus, this simple model appears to describe much of the electro-optical diffraction switching behaviour of these gratings very well, and correlates this behaviour with the observed morphology. Future work will examine the underlying physics more closely.

CONCLUSIONS

The morphology of anisotropically cured polymer dispersed liquid crystalline films has been examined with low-voltage, high-resolution scanning electron microscopy in addition to transmission electron microscopy. The LC concentration had a dramatic effect on the resulting morphology, as 16% LC samples exhibited small, nearly spherical droplets residing in narrow, LC-rich lamellae separated by dense, crosslinked polymer.

Higher concentration samples exhibited much wider LC-rich lamellae with considerable connectivity between the phase-separated droplets. Under the writing conditions employed here, no observable differences in morphology with laser writing intensity were observed. Samples formed under similar writing intensities in an expanded laser geometry showed considerable differences in morphology with intensity, suggesting that the introduction of forced diffusion of LC needs to be considered when discussing polymerization-induced phase separation. The electro-optical behaviour of the gratings was correlated to the observed morphology by a simple model based on slightly elongated LC domains. Switching fields and times, diffraction efficiency and transmission were, to first approximation, predicted using this simple model.

ACKNOWLEDGEMENT

We wish to thank Mr Colin McHugh for assistance with the calculation of volume fractions through image analysis and P. Lloyd for assistance in obtaining the TEM images. The first four authors acknowledge support through Air Force contracts F33600-95-C0055, F33600-93-C0164 and F33615-90-C5911.

REFERENCES

1 Ferguson, J. L. *SID Int. Symp. Dig.* 1985, **16,** 68
2 Doane, J. W., Vaz, N. A., Wu, B.-G J. and Zumer, S. *Appl. Phys. Lett.* 1986, **48,** 269
3 Kitzerow, H. S. *Liq. Cryst.* 1994, **16,** 1
4 Doane, J. W., Golemme, A., West, J. L., Whitehead, J. B. and Wu, B. G. *Mol. Cryst. Liq Cryst.* 1988, **165,** 511
5 Havens, J. R., Leong, D. B. and Reimer, K. B. *Mol. Cryst. Liq. Cryst.* 1990, **178,** 89
6 Lovinger, A. J., Amundson, K. R. and Davis, D. D. *Chem. Mater.* 1994, **6,** 1726
7 Sansone, M. J., Khanarian, G., Leslie, T. M., Stiller, M., Altman, J. and Elizondo, P. *J. Appl. Phys.* 1990, **67,** 4253
8 Lackner, A. M., Margerum, J. D., Ramos, E. and Lim, K. C. *Proc. SPIE* 1989, **1080,** 53
9 Murai, H., Gotoh, T., Suzuki, M., Hasegawa, E. and Mizoguchi, K. *Proc. SPIE* 1992, **1665,** 230
10 Ingwall, R. T. and Adams, T. *Proc. SPIE* 1991, **1555,** 279
11 Ingwall, R. T. and Fielding, H. L. *Opt. Eng.* 1985, **24,** 808
12 Sutherland, R. L., Natarajan, L. V., Tondiglia, V. P., Bunning, T. J. and Adams, W. W. *SPIE Proc.* 1994, **2152,** 303
13 Sutherland, R. L., Natarajan, L. V., Tondiglia, V. P. and Bunning, T. J. *Chem. Mater.* 1993, **5,** 1533.
14 Sutherland, R. L., Tondiglia, V. P., Natarajan, L. V., Bunning, T. J. and Adams, W. W. *Appl. Phys. Lett.* 194, **64,** 1074.
15 Smith, G. W. and Vaz, N. A. *Liq. Cryst.* 1988, **3,** 543
16 Smith, G. W. and Vaz, N. A. *Mol. Cryst. Liq. Cryst* 1993, **237,** 243
17 Vaz, N. A., Smith, G. W. and Montomery, G. P. *Mol. Cryst. Liq. Cryst.* 1987, **146,** 1
18 Krongauz, V. V., Schmelzer, E. R. and Yohannan, R. M. *Polymer* 1991, **32,** 1654
19 Krongauz, V. V. and Legere-Krongauz, C. C. *Polymer* 1993, **34,** 3614
20 Landau, L. D. and Lifshitz, E. M. 'Statistical Physics', Addison Wesley, Reading, MA, 1969
21 Gunton, J. D., Miguel, M. S. and Sahni, P. S. 'Phase Transitions and Critical Phenomena', Academic, London, 1983
22 Olabisi, O., Robeson, L. M. and Shaw, M. T. 'Polymer–Polymer Miscibility', Academic Press, New York, 1979
23 Kogelnik, H. *Bell Syst. Tech. J.* 1969, **48,** 2909
24 Wu, B. G., Erdmann, J. H. and Doane, J. L. *Liq. Cryst.* 1989, **5,** 1453
25 Jacobs, S. D. in 'Handbook of Laser Science and Technology: Opticals Materials; Part 2; (Eds. M. J. Weber), CRC Press, Boca Raton, 1986